nature medicine

Cancer cell–autonomous contribution of type I interferon signaling to the efficacy of chemotherapy

Antonella Sistigu[1–4,35], Takahiro Yamazaki[1–3,35], Erika Vacchelli[1,3,5,35], Kariman Chaba[5–7], David P Enot[5–7], Julien Adam[1,8,9], Ilio Vitale[10], Aicha Goubar[1,11], Elisa E Baracco[1,3,5], Catarina Remédios[1–3], Laetitia Fend[1,2,12], Dalil Hannani[1–3], Laetitia Aymeric[1–3], Yuting Ma[1,3,5], Mireia Niso-Santano[1,3,5], Oliver Kepp[1,3,5], Joachim L Schultze[13], Thomas Tüting[14], Filippo Belardelli[4], Laura Bracci[4], Valentina La Sorsa[4], Giovanna Ziccheddu[4], Paola Sestili[4], Francesca Urbani[4], Mauro Delorenzi[15–17], Magali Lacroix-Triki[18], Virginie Quidville[1,9], Rosa Conforti[1,2,19,20], Jean-Philippe Spano[20], Lajos Pusztai[21], Vichnou Poirier-Colame[1,2,19], Suzette Delaloge[1,8], Frederique Penault-Llorca[22], Sylvain Ladoire[23–25], Laurent Arnould[23–25], Joanna Cyrta[1,8], Marie-Charlotte Dessoliers[1,11], Alexander Eggermont[3], Marco E Bianchi[26], Mikael Pittet[27,28], Camilla Engblom[27,28], Christina Pfirschke[27,28], Xavier Préville[12], Gilles Uzè[29], Robert D Schreiber[30], Melvyn T Chow[31], Mark J Smyth[31,32], Enrico Proietti[4], Fabrice André[1,3,8,9,11,36], Guido Kroemer[1,5–7,33,34,36] & Laurence Zitvogel[1–3,19,36]

Some of the anti-neoplastic effects of anthracyclines in mice originate from the induction of innate and T cell–mediated anticancer immune responses. Here we demonstrate that anthracyclines stimulate the rapid production of type I interferons (IFNs) by malignant cells after activation of the endosomal pattern recognition receptor Toll-like receptor 3 (TLR3). By binding to IFN-α and IFN-β receptors (IFNARs) on neoplastic cells, type I IFNs trigger autocrine and paracrine circuitries that result in the release of chemokine (C-X-C motif) ligand 10 (CXCL10). Tumors lacking Tlr3 or Ifnar failed to respond to chemotherapy unless type I IFN or Cxcl10, respectively, was artificially supplied. Moreover, a type I IFN–related signature predicted clinical responses to anthracycline-based chemotherapy in several independent cohorts of patients with breast carcinoma characterized by poor prognosis. Our data suggest that anthracycline-mediated immune responses mimic those induced by viral pathogens. We surmise that such 'viral mimicry' constitutes a hallmark of successful chemotherapy.

The immune system is routinely confronted with cell death resulting from the physiological turnover of renewable tissues, as well as from pathological insults of several types. We hypothesize the existence of a mechanism that allows the immune system to discriminate between physiological and pathological instances of cell death, but the factors that determine whether cellular demise is perceived as a neutral, tolerogenic or immunogenic event remain unclear[1].

Infectious insults are accompanied by so-called microbe-associated molecular patterns (MAMPs), i.e., viral or bacterial products that activate immune cells through a panel of pattern-recognition receptors (PRRs)[2]. Moreover, intracellular pathogens generally trigger adaptive mechanisms aimed toward the re-establishment of homeostasis, including the unfolded protein response (UPR) and autophagy[3,4]. In mammals, MAMPs coupled to the activation of stress responses

[1]Gustave Roussy Cancer Campus, Villejuif, France. [2]INSERM, U1015, Villejuif, France. [3]Université Paris Saclay, Faculté de Médecine, Le Kremlin Bicêtre, France. [4]Department of Hematology, Oncology and Molecular Medicine, Istituto Superiore di Sanità, Rome, Italy. [5]INSERM, U848, Villejuif, France. [6]Equipe 11 Labellisée par la Ligue Nationale Contre le Cancer, Centre de Recherche des Cordeliers, Paris, France. [7]Université Paris Descartes, Sorbonne Paris Cité, Paris, France. [8]Department of Biology and Pathology, Gustave Roussy Cancer Campus, Villejuif, France. [9]Department of Medical Oncology, Gustave Roussy Cancer Campus, Villejuif, France. [10]Regina Elena National Cancer Institute, Rome, Italy. [11]INSERM, U981, Villejuif, France. [12]Transgene S.A., Illkirch-Graffenstaden, France. [13]Laboratory for Genomics and Immunoregulation, Life and Medical Sciences (LIMES), University of Bonn, Bonn, Germany. [14]Laboratory of Experimental Dermatology, Department of Dermatology, University Hospital Bonn, Bonn, Germany. [15]SIB–Swiss Institute of Bioinformatics, Lausanne, Switzerland. [16]National Center of Competence in Research (NCCR) Molecular Oncology, Institut Suisse de Recherche Expérimentale sur le Cancer (ISREC), School of Life Sciences, École Polytechnique Fédérale de Lausanne (EPFL), Lausanne, Switzerland. [17]Departement de Formation et Recherche, Centre Hospitalier Universitaire Vaudois (CHUV), Lausanne, Switzerland. [18]Department of Pathology, Centre Claudius Regaud, Toulouse, France. [19]Center of Clinical Investigations in Biotherapies of Cancer (CICBT) 507, Villejuif, France. [20]Department of Medical Oncology, Hôpital Pitie Salpetriere, Paris, France. [21]Yale School of Medicine, New Haven, Connecticut, USA. [22]Department of Pathology, Jean Perrin Center, EA 4677 ERTICa, University of Auvergne, Clermont-Ferrand, France. [23]Department of Medical Oncology, Centre Georges-François Leclerc, Dijon, France. [24]INSERM, CRI-866 Faculty of Medicine, Dijon, France. [25]University of Burgundy, Dijon, France. [26]San Raffaele University and Scientific Institute, Milan, Italy. [27]Center for Systems Biology, Massachusetts General Hospital, Boston, Massachusetts, USA. [28]Department of Radiology, Massachusetts General Hospital, Boston, Massachusetts, USA. [29]CNRS UMR5235, University Montpellier II, Place Eugène Bataillon, Montpellier, France. [30]Department of Pathology and Immunology, Washington University School of Medicine, St. Louis, Missouri, USA. [31]Queensland Institute of Medical Research, Herston, Queensland, Australia. [32]School of Medicine, The University of Queensland, Herston, Queensland, Australia. [33]Metabolomics Platform, Gustave Roussy Cancer Campus, Villejuif, France. [34]Pôle de Biologie, Hôpital Européen Georges Pompidou, Assistance Publique–Hôpitaux de Paris (AP-HP), Paris, France. [35]These authors contributed equally to this work. [36]These authors jointly supervised this work. Correspondence should be addressed to L.Z. (laurence.zitvogel@gustaveroussy.fr) or G.K. (kroemer@orange.fr).

Received 5 March; accepted 3 September; published online 26 October 2014; doi:10.1038/nm.3708

are sufficient to render cell death immunogenic[5]. Along similar lines, nonmicrobial instances of cell death, irrespective of whether they are necrotic or apoptotic, can elicit immune responses if they occur in the context of the UPR and autophagy, allowing for the release of endogenous danger signals[1]. Similar to MAMPs, such damage-associated molecular patterns (DAMPs) exert robust, PRR-dependent immunostimulatory effects, rendering cell death immunogenic[6]. Several instances of such an immunogenic cell death (ICD) rely on the UPR-dependent exposure of the reticular chaperone calreticulin on the cell surface, autophagy-dependent secretion of ATP and release of the nuclear protein high mobility group box 1 (HMGB1)[1]. Thus most, if not all, ICD inducers share with pathogenic insults the ability to trigger the UPR and autophagy.

Intriguingly, the anti-neoplastic effects of some chemotherapeutics that are particularly successful in the clinic, including anthracyclines and oxaliplatin, may depend (at least partially) on anticancer immune responses[7]. Thus, the absence of molecular or cellular components of the immune system as well as pharmacological or genetic interventions impeding premortem stress responses, the emission of DAMPs by dying cells or their perception by immune cells blunt the anti-neoplastic effects of ICD inducers in mice[8–11]. Accordingly, DAMP-sensitive PRRs such as TLR4 and purinergic receptor P2X, ligand-gated ion channel, 7 (P2RX7) are important for the response of patients with breast carcinoma to anthracycline-based chemotherapy[11,12]. Moreover, the balance between tumor infiltration by cytotoxic $CD8^+$ and $CD4^+FOXP3^+$ regulatory T cells has substantial predictive value in this context[13].

The aforementioned observations suggest a parallelism between the immunological effects of infection and successful anticancer chemotherapies. Thus, we set out to determine whether type I IFNs, which are essential for communication between virus-infected cells and their noninfected neighbors[14], also participate in chemotherapy-elicited anticancer immunity.

RESULTS

Anthracyclines elicit a type I IFN fingerprint in tumors

To reveal immunologically relevant transcriptional changes induced by chemotherapy, we treated MCA205 fibrosarcomas in mice intratumorally with PBS or doxorubicin, purified $CD45^-$ malignant cells and performed global transcriptome profiling[15]. Doxorubicin induced statistically significant alterations in the levels of MCA205 transcripts, as determined by microarray whole-genome profiling (**Fig. 1a** and **Supplementary Table 1**) and verified by quantitative RT-PCR (qRT-PCR) (**Fig. 1b**). In particular, doxorubicin increased the levels of 18 transcripts associated with viral infections by more than twofold, including (i) several IFN stimulated-genes (ISGs) such as *Rsad2*, which potently inhibits the replication of different viruses[16]; *Oas2*, encoding a template-independent RNA polymerase that generates ribonucleic cofactors for the latent RNase, RNase L[17]; *Mx2*, encoding a large GTPase that has antiviral activity against many RNA viruses[18]; *Dhx58*, a cytoplasmic PRR that senses viral RNA[19]; *Trim30a*, encoding an E3 ligase that inhibits nuclear factor-κB (NF-κB) activation[20]; *Ifit2*, one of the best characterized ISGs[21]; and *Irf7*, encoding a key molecule in type I IFN signaling[22]; (ii) *Ly6C*, *Cxcl10* and *Ccl4*, which are associated with the recruitment or activation of leukocytes[23]; and (iii) *Cd274* (encoding PD-L1), which stimulates PD-1–dependent immunological checkpoints[24]. The levels of other ISG products (such as *Ifi205*, *Mx1*, *Ifnb1*, *Cxcl1* and *Ccl7*) were also increased by three- to tenfold 2 (but not 8) days after the administration of doxorubicin, as determined by qRT-PCR (**Fig. 1b** and **Supplementary Fig. 1a**).

Similar studies performed on GFP-expressing tumors purified by cytofluorometry confirmed that this IFN fingerprint is cancer-cell autonomous (**Fig. 1c**). Moreover, a dozen of the above-mentioned ISGs were upregulated in $CD45^+$ cells 4 days after chemotherapy (**Supplementary Fig. 1b**) but not at an earlier time point (2 days) in several myeloid ($CD11b^+$) cell subsets that are recruited to neoplastic lesions by doxorubicin-based chemotherapy (i.e., $Ly6C^{high}Ly6G^-$, $Ly6C^{low}Ly6G^-$ and $Ly6G^+$ cells)[23] (**Supplementary Fig. 1c**). These results could be extended to several clones of methylcholanthrene (MCA)-induced sarcomas xenografted in histocompatible, wild-type (WT) mice (**Supplementary Fig. 1d**). $CD45^-$ cells extracted from oxaliplatin-treated tumors also contained higher levels of *Ifnb1* transcripts as compared with their PBS-receiving counterparts, as did MCA205 cells exposed to oxaliplatin *in vitro* (**Supplementary Fig. 1e**). These results suggest that neoplastic, not immune, cells engage in a type I IFN response early after exposure to anthracyclines or oxaliplatin.

Cell-autonomous type I IFN responses in chemotherapy

Type I IFNs act on a common receptor, IFNAR, which is composed of two subunits, IFNAR1 and IFNAR2. Doxorubicin reduced the growth of transplantable mammary carcinomas and fibrosarcomas (originating from WT mice) growing in WT or $Ifnar1^{-/-}$ mice to similar extents (**Fig. 1d**). In apparent contrast, Ifnar1-neutralizing antibodies markedly compromised the anti-neoplastic effects of doxorubicin (**Fig. 1e**). In line with this observation, antibodies to both Ifn-α and Ifn-β (Ifn-αβ) and antibodies to Ifnar1 abolished the ability of anthracycline-killed cells to vaccinate mice against viable tumor cells of the same type (**Fig. 1f**). Moreover, two independent MCA-induced sarcomas obtained from $Ifnar2^{-/-}$ mice failed to respond to anthracyclines when implanted into WT mice, whereas *Ifnar2*-sufficient control sarcomas responded normally (**Fig. 2a**). Along similar lines, doxorubicin exerted anti-neoplastic effects against WT MCA205 cells but not against their $Ifnar1^{-/-}$ derivatives (obtained with specific zinc finger nucleases) growing in WT mice (**Supplementary Fig. 2a**).

Notably, $Ifnar1^{-/-}$ cells failed to secrete Cxcl10 or express MHC class I molecules after *in vitro* exposure to recombinant type I Ifn and doxorubicin; yet, when exposed to recombinant Ifn-γ, they expressed similar levels of MHC class I molecules as compared to WT cells (**Supplementary Fig. 2b**,**c**). Together these results indicate that the therapeutic activity of anthracyclines relies on type I IFN signaling in neoplastic, not host, cells.

RNA-sensing PRRs in type I IFN production

Next we exposed a panel of mouse cancer cell lines, including sarcoma, melanoma and leukemia cells, to clinically relevant chemotherapeutic agents that induced their apoptotic demise (**Supplementary Fig. 3a**) and measured the levels of *Ifna2*, *Ifna4*, *Ifnb1* and *Irf7* transcripts by qRT-PCR (**Supplementary Fig. 3b**–**e**). Doxorubicin and mitoxantrone (another anthracycline) readily induced the accumulation of ISG transcripts, whereas mitomycin C and cisplatin (CDDP) failed to do so (**Supplementary Fig. 3b**,**d**,**e**). After exposure to doxorubicin, mouse sarcoma, melanoma and leukemia cells (**Supplementary Fig. 3d**,**e**), as well as human and mouse mammary carcinoma and mouse non–small cell lung carcinoma (NSCLC) cells, expressed a type I IFN fingerprint, thus resembling infection by oncolytic vaccinia viruses[25] (**Supplementary Fig. 4**).

Notably, this response was abolished in MCA-induced sarcomas obtained from mice lacking Tlr3 or its adaptor TLR adaptor molecule 1 (Ticam1, also known as Trif)[14] but not in chemically induced sarcomas lacking IFN induced with helicase C domain 1 (Ifih1), a

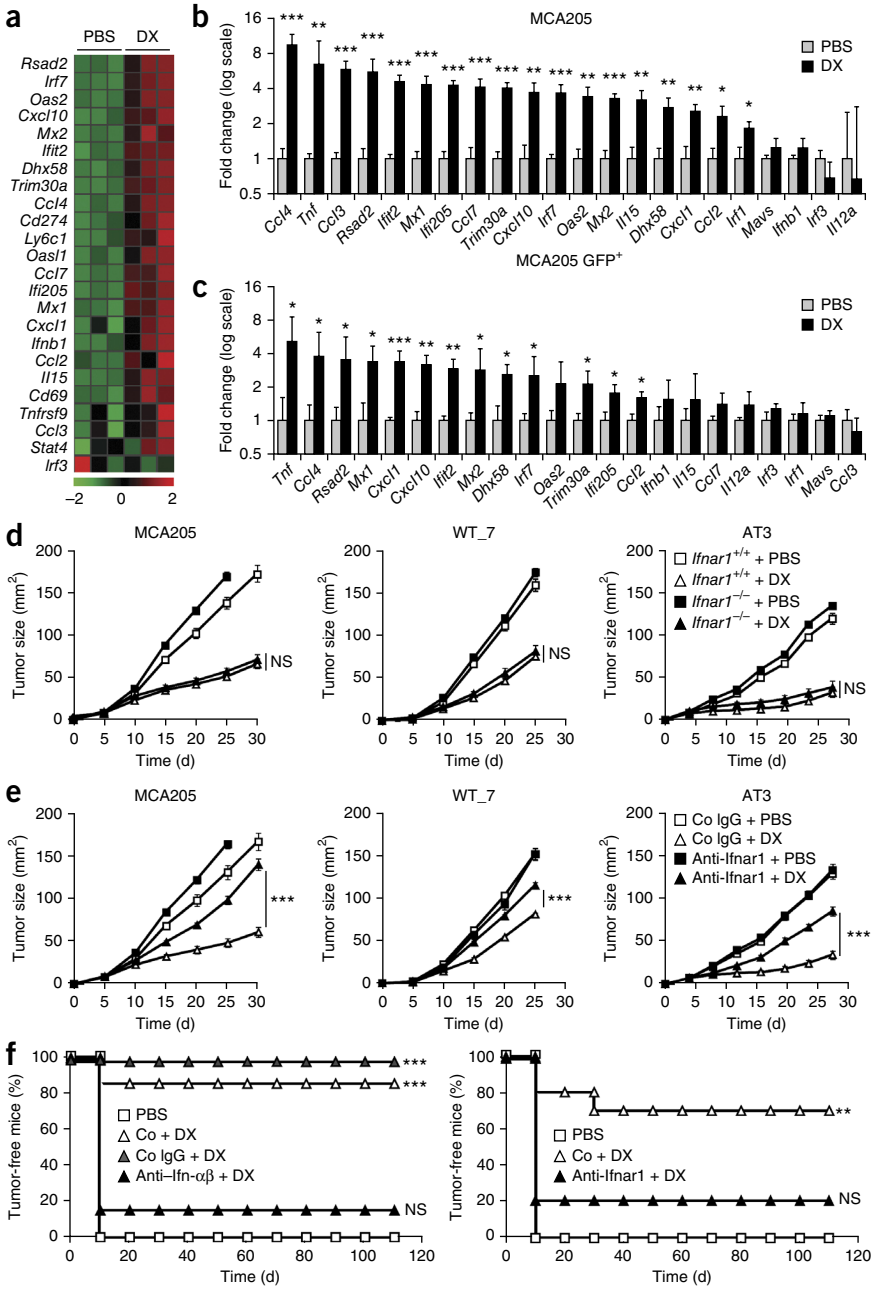

Figure 1 A type I IFN signature in cancer cells is necessary for the therapeutic efficacy of doxorubicin. (**a**) ISG transcripts whose levels in MCA205 fibrosarcomas growing in immunocompetent C57BL/6 mice are increased at least twofold 48 h after a single intratumoral administration of doxorubicin (DX), as determined by transcriptional microarray Illumina whole-genome profiling. (**b**,**c**) Levels of the ISG products in **a** in WT (**b**) and GFP-expressing (**c**) MCA205 fibrosarcomas growing in immunocompetent C57BL/6 mice determined by qRT-PCR analyses of $CD45^-$ (**b**) and GFP^+ (**c**) cells. Data are reported as mean fold changes ±s.e.m. after intrasample normalization to the levels of *Ppia* for n = three animals per group $^*P < 0.05$, $^{**}P < 0.01$, $^{***}P < 0.001$ (unpaired Student's t test) compared to PBS-treated tumors of the same type. (**d**) Tumor size of mouse MCA205 fibrosarcoma, MCA-driven sarcoma WT_7 (a clone from MCA-driven sarcoma grown in WT C57BL/6 mice) and mammary carcinoma AT3 cells that were implanted in WT or *Ifnar1*$^{-/-}$ C57BL/6 mice and treated with either PBS or a single dose of DX intratumorally (i.t.). 8–10 d later. (**e**) Tumor size of MCA205, MCA-WT_7 and AT3 cells that were implanted in WT C57BL/6 mice and treated with PBS or a single dose of DX i.t. in combination with control (Co) IgGs or Ifnar1-neutralizing antibodies 8–10 d later. In **d** and **e**, tumor growth is reported as the mean tumor surface ±s.e.m. over time for n = eight animals per group. One representative experiment out of two yielding similar results is depicted. NS, nonsignificant (unpaired Student's t test) compared to DX-treated tumors growing in WT mice (**d**); $^{***}P < 0.001$ (unpaired Student's t test) compared to tumors treated with DX and control IgGs (**e**). (**f**) DX-exposed MCA205 cells were inoculated into naive mice in the presence or absence of control IgGs, Ifn-αβ–neutralizing antibodies (left) or Ifnar1-neutralizing antibodies (right). Co + DX refers to the solvent of the neutralizing antibody in combination with DX. Control mice received an equivalent volume of PBS as a negative control condition. Tumor incidence in mice rechallenged with living MCA205 cells 1 week later (day 0) is reported for n = 10 animals per group according to the Kaplan-Meier method. NS, nonsignificant. $^{**}P < 0.01$, $^{***}P < 0.001$ (log-rank test) compared to mice vaccinated with DX-treated cells.

cytosolic RNA sensor best known as Mda5 (ref. 26) (**Supplementary Fig. 3c**). In line with this finding, *Ifih1*$^{-/-}$ but not *Tlr3*$^{-/-}$ (generated from mice lacking Tlr3 or obtained with specific zinc finger nucleases) sarcomas responded to anthracycline-based chemotherapy *in vivo* (**Fig. 2a** and **Supplementary Figs. 5** and **6a**), and the absence of *Tlr3* or *Ticam1* (but not *Ifih1*) abolished the ability of doxorubicin to elicit a type I IFN fingerprint in these cells *in vivo* and *in vitro* (**Fig. 2b** and **Supplementary Figs. 1d, 3c** and **6b**). Conversely, the absence of *Rnasel*, coding for an RNase affecting IFN-driven antiviral responses[27], failed to influence the therapeutic activity of anthracyclines (**Fig. 2a** and **Supplementary Fig. 5**). Moreover, although doxorubicin promoted the secretion of Ifn-β1 from WT sarcoma cells, it failed to do so in their *Ifnar2*$^{-/-}$, *Tlr3*$^{-/-}$and *Ticam1*$^{-/-}$ counterparts (**Fig. 2c**). Of note, the exogenous administration of Benzonase (which degrades all nucleic acids) or RNase A, but not RNase H or DNase, significantly reduced the type I IFN transcriptional fingerprint and the secretion of Ifn-β1 and Cxcl10 triggered in living sarcoma cells by their doxorubicin-treated homologous counterparts in coculture experiments (**Fig. 2d**,**e**). These data suggest that anthracyclines stimulate the production of type I IFN through an autocrine and paracrine circuitry involving TLR3 signaling and the emission of self RNA by dying cells.

IFNAR-induced CXCL10 in anthracycline-based chemotherapy

CXCL10 is one of the characteristic chemokines of the type I IFN fingerprint (**Fig. 1a**,**b**) and has a cardinal role in antiviral immune responses[28]. The exposure of mouse sarcoma cells to sublethal amounts of doxorubicin induced the accumulation of *Cxcl10* transcripts, as well as the secretion of Cxcl10 and Ccl5 (**Fig. 3a**,**b** and **Supplementary Fig. 7a**,**b**) but not Ccl3 (data not shown). However,

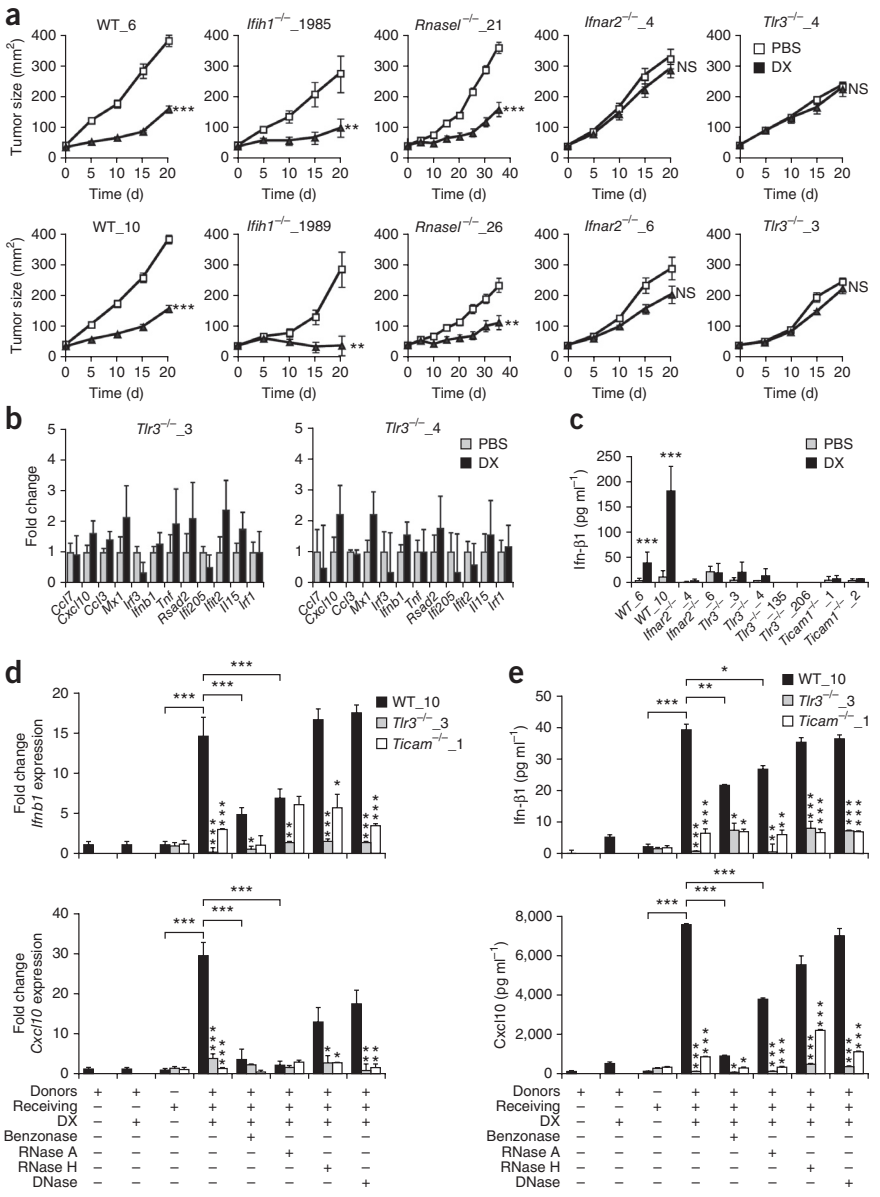

Figure 2 TLR3-TICAM1 signaling is required for type I IFN release by cancer cells. (**a**) Tumor growth of MCA-driven sarcomas of the indicated genotypes established in WT C57BL/6 mice ($n = 10$ per group) that were treated with PBS or a single intratumoral injection of DX. Tumor growth is reported as the mean tumor surface ±s.e.m. over time. NS, nonsignificant. $^{**}P < 0.01$, $^{***}P < 0.001$ (unpaired Student's *t* test) compared to PBS-treated tumors. (**b**) Expression levels of ISG products in the CD45$^-$ fraction of two distinct *Tlr3*$^{-/-}$ MCA-driven sarcomas (MCA-*Tlr3*$^{-/-}$_3 and MCA-*Tlr3*$^{-/-}$_4) established in WT C57BL/6 mice ($n = 3$ per group) in response to a single intratumoral injection of DX. Data are reported as mean fold changes ±s.e.m. after intrasample normalization to the levels of *Ppia*. A representative experiment out of two yielding similar results is shown. (**c**) ELISA quantification of extracellular Ifn-β1 in MCA-driven sarcoma cells of the indicated genotypes that were exposed to DX and Tlr4L for 24 h. Data are reported as the means ±s.e.m. $^{***}P < 0.001$ (unpaired Student's *t* test) compared to PBS-treated cells of the same genotype. (**d**,**e**) Quantification of *Ifn1b* and *Cxcl10* levels by qRT-PCR (**d**) and Ifn-β1 and Cxcl10 levels by ELISA (**e**) in MCA-driven sarcoma cells (donor cells) that were left untreated or exposed to DX alone or in the presence of the indicated nucleases for 12 h, after which they were co-incubated with untreated cells of the same type (receiving cells of the indicated genotype) for 12 or 24 h. Data are reported as mean fold changes ±s.e.m. after intrasample normalization to the levels of *Ppia* in two independent experiments (**d**) or pg ml^{-1} ±s.e.m. of triplicate wells from one representative experiment out of three performed yielding similar results (after normalization, when required) (**e**). $^{*}P < 0.05$, $^{**}P < 0.01$, $^{***}P < 0.001$ (unpaired Student's *t* test) compared to WT receiving cells incubated with DX-treated donor cells, *Tlr3*$^{-/-}$ receiving cells incubated with DX-treated donor cells or *Ticam1*$^{-/-}$ receiving cells incubated with DX-treated donor cells.

although recombinant Ifn-α promoted the secretion of Cxcl10, and the doxorubicin-triggered release of Cxcl10 was abolished by antibodies to Ifn-αβ and Ifnar1, neither of these observations held true for Ccl5 (**Supplementary Fig. 7a**,**b**), excluding Ccl5 as a downstream effector of anthracycline-dependent type I IFN responses. Doxorubicin and mitoxantrone also promoted the release of CXCL10 from mouse and human mammary carcinoma cells, as well as from mouse NSCLC cells (**Supplementary Fig. 7c**,**d**).

Unlike their WT and *Ifih1*$^{-/-}$ counterparts, *Ifnar2*$^{-/-}$, *Tlr3*$^{-/-}$ and *Ticam1*$^{-/-}$ sarcoma cells not only failed to respond to doxorubicin *in vivo* (**Fig. 2a**) but also did not secrete Cxcl10 after exposure to doxorubicin *in vitro* (**Fig. 3b**), correlating with their inability to generate type I IFN responses (**Fig. 2b**,**c** and **Supplementary Fig. 3c**). Notably, the chemosensitivity of *Ifnar2*$^{-/-}$ and *Tlr3*$^{-/-}$ (but not WT) sarcomas was restored by intratumoral inoculation of recombinant Cxcl10 (**Fig. 3c**) but not Ccl4 (**Fig. 3d**). Moreover, WT tumors failed to respond to doxorubicin in the presence of antibodies neutralizing Cxcr3, the main Cxcl10 receptor (**Fig. 3e**). These results emphasize the functional relevance of the Cxcl10-Cxcr3 signaling axis operating downstream of Tlr3 and Ifnar for the therapeutic efficacy of anthracyclines.

Chemosensitizing effects of type I IFN

Intratumoral administration of purified Ifn-αβ restored the chemotherapeutic response to doxorubicin in *Tlr3*$^{-/-}$ but not *Ifnar2*$^{-/-}$ sarcomas growing in WT mice (**Fig. 4a**). These data corroborate the notion that optimal chemotherapeutic responses rely on type I IFN signaling in neoplastic cells. We thus set out to determine whether an exogenous supply of Ifn-αβ would improve the anticancer immune responses elicited by CDDP-killed cancer cells, knowing that this agent is intrinsically unable to stimulate type I IFN secretion (**Supplementary Fig. 3b**,**d**,**e**). We found that exogenous Ifn-αβ (but not Ifn-γ) greatly enhanced the ability of CDDP-treated MCA205 and ovalbumin (OVA)-expressing B16 melanoma cells to induce protective antitumor immune responses in immunocompetent mice (**Fig. 4b**,**c**).

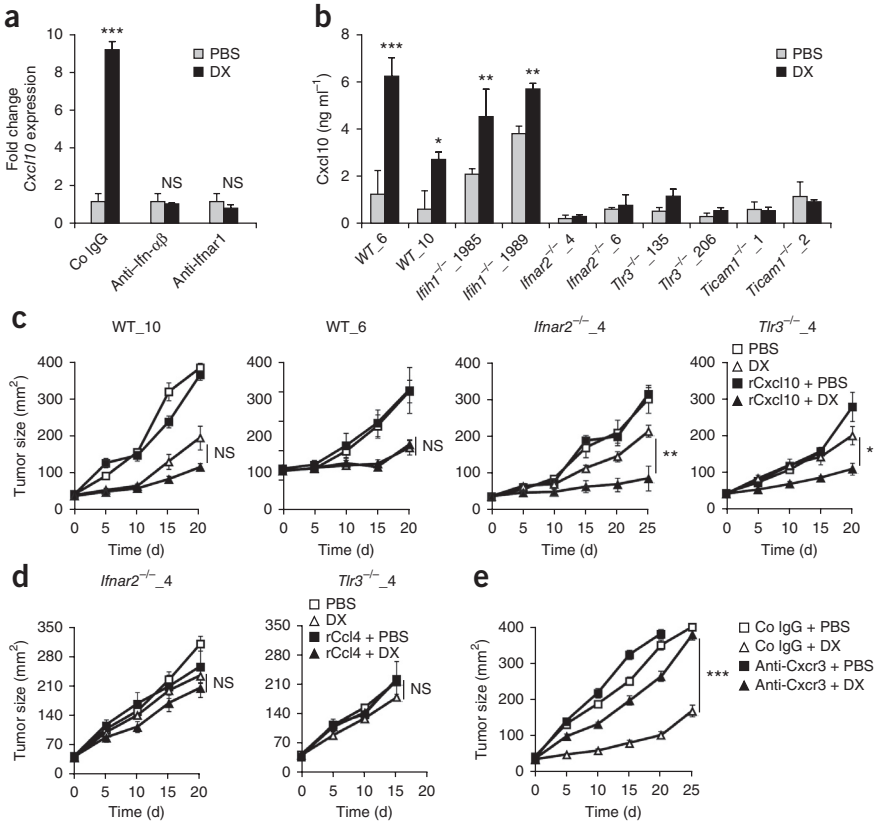

Figure 3 Role of CXCL10 in the anti-neoplastic activity of anthracyclines. (**a**) Quantification of *Cxcl10* levels by qRT-PCR in WT MCA205 fibrosarcoma cells that were treated with PBS or DX in the presence of control (Co) IgGs, Ifn-αβ–neutralizing antibodies or Ifnar1-neutralizing antibodies for 24 h. Data are reported as mean fold changes ±s.e.m. after intrasample normalization to the levels of *Ppia*. One representative experiment out of two yielding similar results is depicted. NS, nonsignificant. $***P < 0.001$ (unpaired Student's *t* test) as compared to PBS for DX-treated cells or as compared to DX treatment alone for cells treated with DX plus antibodies to either Ifn-αβ or Ifnar. (**b**) ELISA quantification of extracellular Cxcl10 in MCA-driven sarcoma cells of the indicated genotypes that were exposed to DX for 24 h. Data are reported as means ±s.e.m. Concatenated data from two independent experiments are depicted. $*P < 0.05$, $**P < 0.01$, $***P < 0.001$ (unpaired Student's *t* test) compared to PBS-treated cells of the same genotype. (**c**,**d**) Tumor size of MCA-driven sarcomas of the indicated genotypes established in WT C57BL/6 mice ($n = 10$ per group) that were treated with PBS or a single intratumoral injection of DX alone or in combination with recombinant Cxcl10 (rCxcl10, **c**) or recombinant Ccl4 (rCcl4, **d**). $*P < 0.05$, $**P < 0.01$, (**e**) Tumor size of WT MCA205 fibrosarcomas established in C57BL/6 mice ($n = 10$ per group) that were treated with PBS or a single intratumoral injection of DX in combination with control IgG or Cxcr3-neutralizing antibodies. In **c**–**e**, tumor growth is reported as the mean tumor surface ±s.e.m. over time. NS, nonsignificant. $***P < 0.001$ (unpaired Student's *t* test) compared to DX-treated tumors.

On a similar note, the anti-neoplastic potential of CDDP against fibrosarcoma cells was significantly improved by Ifn-αβ and recombinant Cxcl10 but not by recombinant Ccl4 in both induction and regression settings in which we initiated treatment when WT MCA205 fibrosarcomas had reached a surface area of approximately 50 mm^2 (**Fig. 4d**,**e**). Notably, the chemosensitizing potential of Ifn-αβ was not compromised by an absence of *Ifnar2* from the host (**Fig. 4e**), again confirming that type I IFN enhances chemotherapeutic responses by acting on malignant cells rather than on immune or nonimmune host compartments. These data suggest that an exogenous supply of IFN-αβ can exert chemosensitizing effects when malignant cells bear an intact IFNAR signaling cascade.

MX1 predicts clinical response in patients with breast carcinoma

On the basis of our preclinical findings, we set out to determine whether IFN responses could define a subset of patients with breast carcinoma (BC) that are sensitive to anthracyclines. We first assessed whether the type I IFN metagene (a transcriptional signature centered around the expression of *MX1*) and other previously defined metagenes would predict the efficacy of neoadjuvant anthracycline-based chemotherapy in a cohort of 24 responding patients with BC paired with 26 nonresponders that shared classical clinical predictors[29]. Unlike other metagenes (such as *TPX2*, *ESR1*, *CLCA2*, *ADM*, *FABP4*, DCN, *GZMA*, *CD83*, see **Supplementary Table 3**), the *IFN* metagene predicted the occurrence of pathological complete response (pCR) in both estrogen receptor (ER)-negative individuals (area under the ROC curve (AUC) = 0.74, 95% confidence interval (CI) 0.57–0.89, $P = 0.004$) and the overall patient population (AUC = 0.72, 95% CI 0.57–0.86, $P = 0.004$) (**Fig. 5a** and **Supplementary Tables 2** and **3**). Next we searched for publicly available transcriptomic studies focusing on patients with BC who were treated with anthracyclines alone or in combination with taxane-based neoadjuvant chemotherapy. We identified six such studies that involved a total of 1,320 patients (GSE6861 and refs. 30–34). We assessed the predictive value of *MX1* and *TLR3* probe sets by the AUC method in datasets from each of these studies and found that *MX1* expression at diagnosis was associated with an increased likelihood of pCR in all cohorts but one (cohort 3, ref. 32) (**Fig. 5b**). Moreover, we observed that expression levels of *MX1* correlated with those of *CXCL10* and, to a lesser extent, *TLR3* (**Fig. 5b**). *TLR3* expression had no predictive power with regard to the probability of pCR.

To demonstrate that anthracyclines promote the expression of MX1 in human tumors, we developed a specific immunohistochemical procedure for the staining of serial, paraffin-embedded BC biopsies (**Fig. 5c**). On the basis of correlations between the *IFN* metagene and immunohistochemical data, we determined the clinically relevant cutoff of MX1 levels measured as Allred scores integrating staining intensity and the fraction of MX1-expressing malignant cells[35]. We found that MX1 Allred scores significantly increased 3 weeks after one cycle of chemotherapy (**Fig. 5c**,**d**). However, a positive correlation persisted between MX1 Allred scores before and after chemotherapy (**Fig. 5e**), suggesting that measurement of MX1 levels at diagnosis might reflect the capacity of BC to mount a type I IFN response to therapy.

We employed this approach to analyze MX1 expression in a cohort of 743 patients with BC who we randomly allocated to anthracycline-based adjuvant chemotherapy or no chemotherapy[36] (**Fig. 6a**). MX1 was expressed at high levels (MX1 Allred score >6) in 93 (12%)

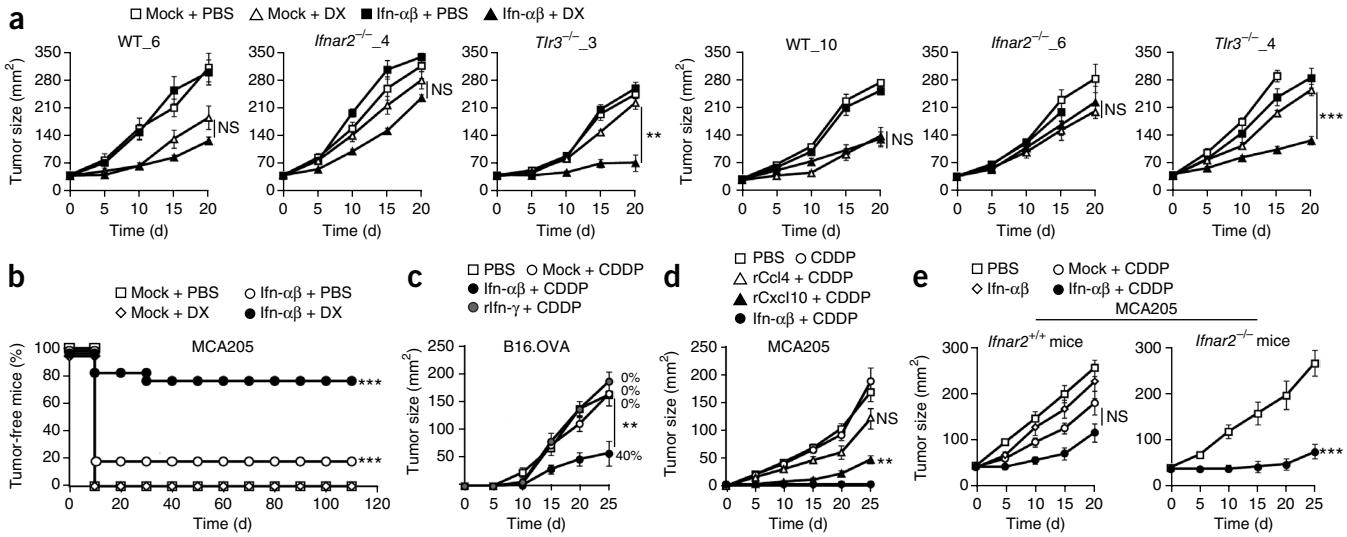

Figure 4 Improvement of chemotherapeutic responses by exogenous type I IFN. (**a**) Tumor size of MCA-driven sarcomas of the indicated genotypes established in WT C57BL/6 mice (n = ten per group) that were treated with PBS or a single intratumoral injection of DX in combination with purified Ifn-αβ or an appropriate control (a mock preparation from untreated cells not containing Ifn-αβ). Tumor growth is reported as the mean tumor surface ±s.e.m. over time. NS, not significant. $^{**}P < 0.01$, $^{***}P < 0.001$ (unpaired Student's t test) compared to DX-treated tumors. (**b**,**c**) WT fibrosarcoma MCA205 cells (**b**) and OVA-expressing B16 (B16.OVA) melanoma cells (**c**) were exposed to CDDP *in vitro* and inoculated into naive mice alone or in the presence of Ifn-αβ, an appropriate control (a mock preparation from untreated cells not containing Ifn-αβ) or recombinant Ifn-γ (rIfn-γ). Control mice received an equivalent volume of PBS as a negative control condition. Tumor incidence (**b**) and tumor growth kinetics (**c**) in mice rechallenged with living MCA205 or B16.OVA cells 1 week later (day 0) is reported for $n = 10$ animals per group according to the Kaplan-Meier method. Tumor growth is reported as the mean tumor surface ±s.e.m. over time. $^{**}P < 0.01$, $^{***}P < 0.001$ (log-rank test in **b**, unpaired Student's t test in **c**) compared to mice vaccinated with CDDP-treated cells. The percentages on the right of the plot in **c** indicate the percentage of tumor-free mice at the end of the experiment. (**d**,**e**) Tumor size of MCA205 fibrosarcomas established in WT or *Ifnar2*$^{-/-}$ C57BL/6 mice (ten per group) that were treated with PBS or intratumoral CDDP, alone or combined with Ifn-αβ, an appropriate control (supernatant from untreated cells), rCxcl10 or rCcl4. Tumor growth is reported as the mean tumor surface ±s.e.m. over time. NS, nonsignificant. $^{**}P < 0.01$, $^{***}P < 0.001$ (unpaired Student's t test) compared to CDDP-treated tumors (**d**,**e**).

samples (**Supplementary Table 4**). In this setting, adjuvant chemotherapy was associated with a nonsignificant reduction in the death rate of the overall population (adjusted hazard ratio (HR) = 0.90, 95% CI 0.67–1.21, $P = 0.5$), and ER positivity, as determined by a ligand binding assay, did not convey predictive information (interaction test, $P = 0.22$). In a Cox model calculated on 645 patients integrating ER status, lymph node involvement, histological grade and treatment arm, adjuvant chemotherapy was associated with a reduction in the death risk of patients with MX1^{high} neoplasms (adjusted HR = 0.42, 95% CI 0.18–1.01) but not in patients bearing MX1^{low} tumors

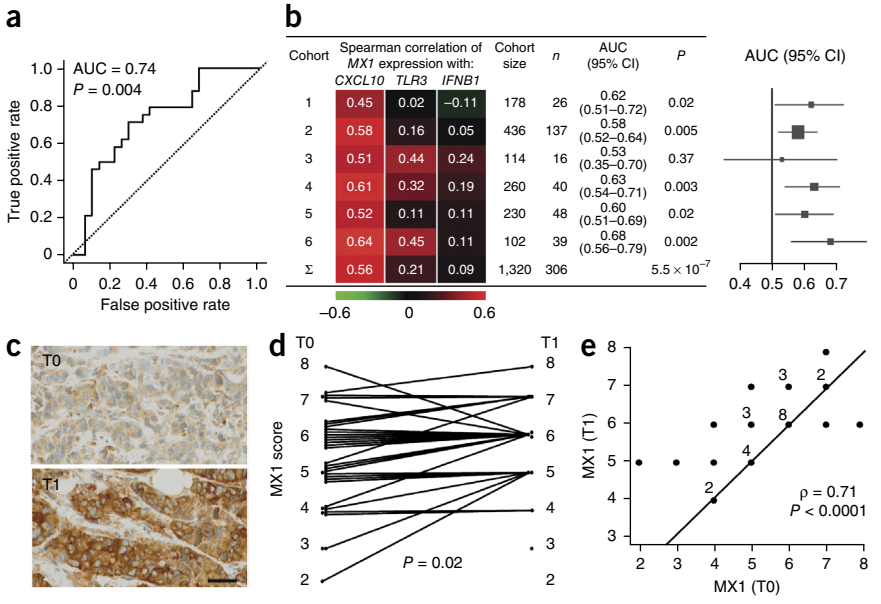

Figure 5 *MX1* expression in BC predicts pCR to neoadjuvant anthracycline-based chemotherapy. (**a**) Microarray-based *MX1* expression data and pCR in 24 patients with BC treated with neoadjuvant anthracycline-based chemotherapy at the Gustave Roussy Cancer Campus determined by the AUC method. (**b**) Microarray-based *MX1* expression data from six publicly available cohorts of patients with BC treated with neoadjuvant anthracycline-based chemotherapy, *CXCL10*, *TLR3* and *IFNB1* expression levels (determined by the Spearman method) and pCR (determined by the AUC method). n, number of responders. P value calculations for **a** and **b** are described in the Online Methods. (**c**–**e**) MX1 expression levels quantified by Allred score after staining with a MX1-specific antibody in paraffin-embedded biopsies obtained from 33 patients with BC before (T0) and 3 weeks after one cycle of anthracycline-based chemotherapy (T1) (and in four patients either before or after one cycle). (**c**) Representative images of MX1-negative (Allred score <6, T0) and MX1-positive (Allred score ≥6, T1) tumor slices. The scale bar indicates 100 µm. (**d**) Allred scores of 33 paired (T0 and T1) and eight unpaired (four T0 and four T1) biopsies. Statistical significance was determined by Wilcoxon signed-rank test. (**e**) Correlation of the expression levels of MX1 at T0 and T1 in **e**. Numbers indicate how many patients coincided at each point with identical values.

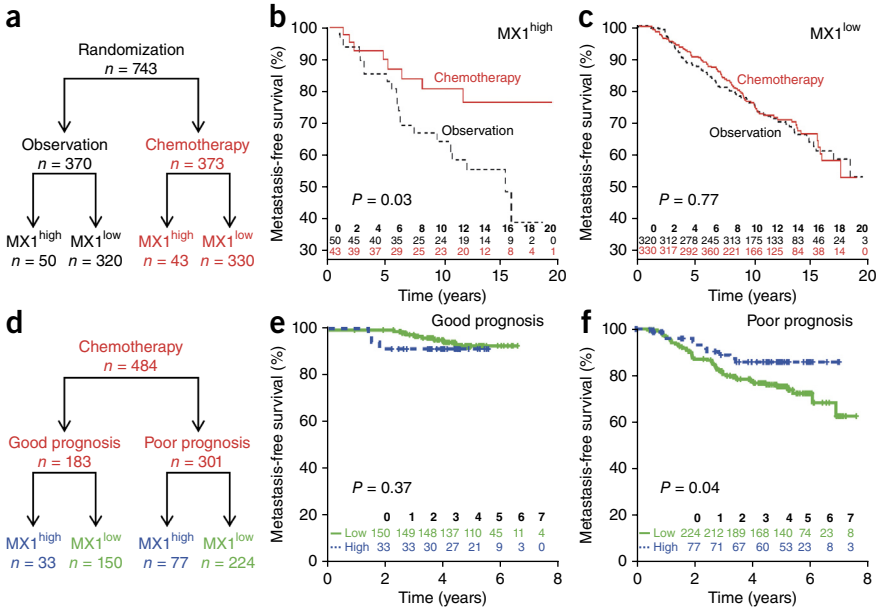

Figure 6 Predictive value of *MX1* expression in patients with BC treated with adjuvant chemotherapy. (**a**) Clinical and analytical protocol in a study investigating MFS in patients with BC treated with adjuvant chemotherapy in a randomized French study. (**b**,**c**) MFS of patients bearing BC according to their MX1 Allred score after stratification by status of adjuvant chemotherapy receiver. Statistical significance was determined by log-rank test. The red and black numbers show the number of patients at risk in each treatment group (chemotherapy or observation alone, respectively) for distinct observation times (bold numbers indicating years post surgery). (**d**) Clinical and analytical protocol for investigating the predictive value of MX1 expression in patients with BC with poor prognosis (484 TMAs were available for MX1 immunohistochemistry and clinical parameters). (**e**,**f**) MFS of patients bearing BC with good (**e**) or poor (**f**) prognosis after stratification by MX1 expression levels. Poor prognosis was defined by the presence of one or more of the following clinical characteristics: tumor grade III, more than three lymph nodes involved and ER negativity. Statistical significance was determined by log-rank test. The number of patients at risk in each group (green, low expression; blue, high expression) are reported. $MX1^{high}$ was defined by Allred score ≥6. *P* values were calculated by means of Cox and bias-corrected Cox models.

(HR = 1.01, 95% CI 0.74–1.38). The 15-year overall survival (OS) rate of patients bearing $MX1^{high}$ BC treated with adjuvant anthracycline-based chemotherapy was 77% (95% CI 56–88%), whereas that of untreated patients with $MX1^{high}$ tumors was 56% (95% CI 39–69%) (**Fig. 6b**). In contrast, 15-year OS rates were similar (66%, 95% CI 59–72%) for patients bearing $MX1^{low}$ carcinomas irrespective of chemotherapy (**Fig. 6c**).

We next evaluated the predictive value of MX1 expression according to ER status. Adjusted HRs for death associated with the use of adjuvant chemotherapy were 0.37 (95% CI 0.13–1.03), 0.85 (95% CI 0.40–1.79), 0.45 (95% CI 0.18–1.12) and 1.05 (95% CI 0.75–1.46) for individuals with $ER^{-}MX1^{high}$ ($P = 0.06$), $ER^{-}MX1^{low}$ ($P = 0.67$), $ER^{+}MX1^{high}$ ($P = 0.09$) and $ER^{+}MX1^{low}$ ($P = 0.79$) BC, respectively. To corroborate these findings, we analyzed 487 samples selected randomly out of 1,646 tissue microarrays (TMAs) available from 3,010 patients with early breast carcinoma presenting with nodal involvement in the context of the PACS04 phase 3 clinical trial (NCT00054587) for *MX1* (available on 487 TMAs) and *TLR3* (available on 337 TMAs) expression. This study aimed to compare six cycles of 5-fluorouracil–, epirubicin- and cyclophosphamide-based chemotherapy to six cycles of a regimen involving epirubicin plus docetaxel (followed by trastuzumab in $ERBB2^{+}$ patients)[37] (**Supplementary Fig. 8**). On the basis of the Allred scoring system, 22.5% (110/487) of these patients had $MX1^{high}$ neoplasms, thus positively associating this type of neoplasm with high tumor grade (**Supplementary Table 5**). This prompted us to categorize the cohort on the basis of the presence of at least one clinical parameter associated with poor prognosis (Scarff-Bloom-Richardson grade III, more than three metastatic axillary lymph nodes or ER negativity) (**Fig. 6d**). Of note, in three cases, grade was not available, restricting the analysis to 484 patients with BC. In the patients with favorable prognosis, MX1 expression levels failed to affect metastasis-free survival (MFS) (**Fig. 6e**). Conversely, in patients with poor prognosis, high MX1 levels were associated with increased MFS, pointing to a positive interaction with chemotherapy (**Fig. 6f**). Although there was strong intraspecimen correlation between *TLR3* and *MX1* expression levels as evaluated by immunohistochemistry (**Supplementary Fig. 9**), TLR3 expression failed to accurately predict MFS (**Supplementary Table 6**). Together these results suggest that robust *MX1* expression predisposes patients with BC who have poor prognosis to improved chemotherapeutic responses to anthracycline-based chemotherapy.

DISCUSSION

Viral infection culminates in the secretion of type I IFNs, bridging innate and adaptive antiviral immune responses[38]. Here we demonstrate that anthracyclines mimic viral infection, as they stimulate RNA sensors in neoplastic cells, eliciting an autocrine and paracrine type I IFN→IFNAR→CXCL10 signaling pathway that underlies optimal chemotherapeutic responses. We implicated TLR3 (an endosomal RNA sensor)[39] but neither IFIH1 (a cytosolic RNA sensor)[27] nor RNASEL (a cytosolic RNase) in the apical signal transduction of this pathway.

The ability of anthracyclines to mimic viral infection appears to involve (at least partially) the release of self RNA by stressed or dying cancer cells. Thus, Benzonase (a general nuclease) and RNase A (which degrades mainly single-stranded RNA) destroyed an as-yet-unknown ligand of TLR3, which is best known as a double-stranded RNA sensor but has also been reported to recognize single-stranded RNA[40]. However, the biochemical structure of the anthracycline-elicited TLR3 ligand and its cellular source remain to be determined. Several DNA-damaging agents stimulate TLR3 expression[41], and some of them have been shown to generate double-stranded RNAs that can activate TLR3-dependent secretion of cytokines[42]. Synthetic TLR3 agonists are known to exert both cancer cell–intrinsic and immune system–dependent anti-neoplastic effects in preclinical[43,44] as well as clinical[45] settings. In line with our findings, the therapeutic activity of TLR3 ligands requires CXCL10 (ref. 46). However, the impact of CXCL10 on the immune system and, in particular, on tumor-infiltrating T lymphocytes remains to be determined.

Clearly both type I and type II IFNs are required for anticancer immune responses elicited by anthracyclines *in vivo*. However, type I IFNs are produced by cancer cells 1–4 days after chemotherapy, coinciding with the accumulation of autophagic and dying cells within neoplastic lesions[9], as well as with the first wave of tumor infiltration by myeloid cells[23]. Moreover, type I IFNs appear to contribute to chemotherapeutic responses by operating on neoplastic, rather than host, cells. Conversely, IFN-γ is not detectable until 5 days after chemotherapy and is produced exclusively by $CD45^+$ cells, mostly α/β T helper type 1 or cytotoxic type 1 T lymphocytes[10,11]. Thus, there are major functional differences in the contribution of type I and type II IFNs to chemotherapy-induced immunosurveillance.

Of note, chemically induced cancers arise at a higher frequency and more rapidly in *Ifnar1*$^{-/-}$ than *Ifnar1*$^{+/+}$ mice[47,48]. Moreover, genetic variants in type I IFN–coding genes influence the clinical outcome of patients with melanoma[49]. However, type I IFN contributes to natural anticancer immunosurveillance, mostly through CD8-α^+ dendritic cells[50,51]. Conversely, the ability of anthracyclines to promote ICD relies mainly on inflammatory monocytes developing into *bona fide* dendritic cells through a purinergic receptor P2Y, G-protein coupled 2 (P2RY2)-dependent pathway[23]. Thus, some of the mechanisms underlying natural and chemotherapy-induced immunosurveillance differ, including the cellular target of type I IFNs.

IFN-related chemokines have a major role in tumor infiltration by T cells[52], and chemokine gradients can be altered by chemotherapy. The administration of temozolomide reportedly promotes the release of CXCR3-binding chemokines by mouse and human melanomas, correlating with T cell infiltration[53]. This may imply that recombinant IFN-α_{2b}, an inducer of CXCL9 and CXCL10 that is approved for the treatment of high-risk melanoma[54], might exert anti-neoplastic effects at least partially through the release of CXCR3 ligands.

Our findings may have important clinical implications. Tumor infiltration by immune cells indeed influences disease outcome in patients with BC at both the prognostic[55,56] and predictive levels[57]. We observed that *MX1* expression correlates positively with tumor grade and was upregulated by the first cycle of chemotherapy, in concordance with previous observations[58]. Notably, a type I IFN metagene centered around *MX1* constitutes a predictive biomarker of pCR to neoadjuvant anthracycline-based chemotherapy in BC. Moreover, in the subset of patients with BC with poor prognosis, *MX1* expression by tumor cells predicted metastasis-free survival after adjuvant chemotherapy. In contrast, *TLR3* expression had no predictive power with regard to the outcome of breast cancer treatments, in line with the idea that the downstream elements of the cascade (MX1 is downstream of IFNAR) constitute better biomarkers than the initiating events.

On the basis of the preclinical and clinical data reported here, we speculate that molecular defects in any of the molecules involved in TLR3-elicited, type I IFN–dependent, IFNAR-transduced signaling pathways[59] may compromise the therapeutic efficacy of anthracyclines. We surmise that patients bearing such tumors might benefit from the targeted delivery of type I IFN[60] or CXCL10.

METHODS

Methods and any associated references are available in the online version of the paper.

Note: Any Supplementary Information and Source Data files are available in the online version of the paper.

ACKNOWLEDGMENTS

We acknowledge L. Galluzzi for help with preparation of the manuscript. We thank P. Rameau, Y. Lécluse and M. Sanchez for assistance with FACS experiments, G. Schiavoni and G. D'Agostino (Istituto Superiore di Sanità) for recombinant Ifn-α1, our colleagues from the Gustave Roussy Cancer Center and the Istituto Superiore di Sanità animal facilities, P. Gonin, M. Macchia and E. Cardarelli. We acknowledge P. Vielh for his help with immunohistochemical analyses and G. Stoll for his support in statistical analyses. G.K. and L.Z. are supported by the Ligue Nationale contre le Cancer (Equipes labellisées), Site de Recherche Intégrée sur le Cancer (IRIC) Socrates, the ISREC Foundation, Agence Nationale pour la Recherche (ANR AUTOPH, ANR Emergence), the European Commission (ArtForce), a European Research Council Advanced Investigator Grant (to G.K.), the Fondation pour la Recherche Médicale (FRM), the Institut National du Cancer (INCa), the Fondation de France, Cancéropôle Ile-de-France, the Fondation Bettencourt-Schueller, the LabEx Immuno-Oncology and the Paris Alliance of Cancer Research Institutes. A.S. is supported by Ligue Nationale contre le Cancer. D.H. was supported by Fondation Association pour la Recherche sur le Cancer. M.J.S. was supported by a National Health and Medical Research Council (NH&MRC) Australia Fellowship and Program Grant and a grant from the Victorian Cancer Agency. E.P. and L.B. were supported by Associazione Italiana Ricerca contro il Cancro (AIRC) (MFAG_13058). C.P. was supported by the Deutsche Forschungsgemeinschaft (DFG) PF809/1-1. C.E. was supported by Boerhinger Ingelheim. F.A. was supported by Association Vie et Cancer. J.A. was supported by Institut national du Cancer et la Direction Générale de l'Offre de Soins-INSERM 6043.

AUTHOR CONTRIBUTIONS

A.S., T.Y., E.V., K.C., I.V., E.E.B., C.R., L.F., D.H., L. Aymeric, Y.M., M.N.-S., O.K., J.L.S., V.L.S., G.Z., P.S., F.U., M.P., C.E., C.P., M.J.S. and M.T.C. performed experiments. M.D., V.Q., R.C., J.-P.S., L.P., S.D., A.E. and F.A. enrolled patients in clinical trials. F.B., L.B. and E.P. directed part of A.S.'s experiments and supported the fees of the animal work. F.B., T.T., M.E.B., G.U. and R.D.S. provided reagents. L.Z. daily directed the two first authors and conceived the study. L.Z., F.A. and G.K. wrote the paper. V.P.-C. processed the TMAs and performed immunostaining of the biopsies and TMAs. A.G. and D.P.E. performed statistical analyses. J.A., S.L., L. Arnould, J.C., M.-C.D., F.P.-L. and M.L.-T. were the pathologists who interpreted the MX1 and TLR3 staining. X.P. and L.F. performed the experiments with transgenic oncolytic viruses.

COMPETING FINANCIAL INTERESTS

The authors declare no competing financial interests.

1. Kroemer, G., Galluzzi, L., Kepp, O. & Zitvogel, L. Immunogenic cell death in cancer therapy. *Annu. Rev. Immunol.* **31**, 51–72 (2013).
2. Tang, D., Kang, R., Coyne, C.B., Zeh, H.J. & Lotze, M.T. PAMPs and DAMPs: signal 0s that spur autophagy and immunity. *Immunol. Rev.* **249**, 158–175 (2012).
3. Hetz, C., Martinon, F., Rodriguez, D. & Glimcher, L.H. The unfolded protein response: integrating stress signals through the stress sensor IRE1a. *Physiol. Rev.* **91**, 1219–1243 (2011).
4. Levine, B., Mizushima, N. & Virgin, H.W. Autophagy in immunity and inflammation. *Nature* **469**, 323–335 (2011).
5. Zitvogel, L., Kepp, O. & Kroemer, G. Decoding cell death signals in inflammation and immunity. *Cell* **140**, 798–804 (2010).
6. Matzinger, P. The danger model: a renewed sense of self. *Science* **296**, 301–305 (2002).
7. Zitvogel, L., Kepp, O. & Kroemer, G. Immune parameters affecting the efficacy of chemotherapeutic regimens. *Nat. Rev. Clin. Oncol.* **8**, 151–160 (2011).
8. Panaretakis, T. *et al.* Mechanisms of pre-apoptotic calreticulin exposure in immunogenic cell death. *EMBO J.* **28**, 578–590 (2009).
9. Michaud, M. *et al.* Autophagy-dependent anticancer immune responses induced by chemotherapeutic agents in mice. *Science* **334**, 1573–1577 (2011).
10. Ma, Y. *et al.* Contribution of IL-17–producing γδ T cells to the efficacy of anticancer chemotherapy. *J. Exp. Med.* **208**, 491–503 (2011).
11. Ghiringhelli, F. *et al.* Activation of the NLRP3 inflammasome in dendritic cells induces IL-1β–dependent adaptive immunity against tumors. *Nat. Med.* **15**, 1170–1178 (2009).
12. Apetoh, L. *et al.* The interaction between HMGB1 and TLR4 dictates the outcome of anticancer chemotherapy and radiotherapy. *Immunol. Rev.* **220**, 47–59 (2007).
13. Senovilla, L. *et al.* An immunosurveillance mechanism controls cancer cell ploidy. *Science* **337**, 1678–1684 (2012).
14. González-Navajas, J.M., Lee, J., David, M. & Raz, E. Immunomodulatory functions of type I interferons. *Nat. Rev. Immunol.* **12**, 125–135 (2012).

15. Ma, Y. *et al.* CCL2/CCR2-dependent recruitment of functional antigen-presenting cells into tumors upon chemotherapy. *Cancer Res.* **74**, 436–445 (2014).
16. Lim, E.S., Wu, L.I., Malik, H.S. & Emerman, M. The function and evolution of the restriction factor Viperin in primates was not driven by lentiviruses. *Retrovirology* **9**, 55 (2012).
17. Hovanessian, A.G. *et al.* Identification of 69-kd and 100-kd forms of 2–5A synthetase in interferon-treated human cells by specific monoclonal antibodies. *EMBO J.* **6**, 1273–1280 (1987).
18. Horisberger, M.A. Interferons, Mx genes, and resistance to influenza virus. *Am. J. Respir. Crit. Care Med.* **152**, S67–S71 (1995).
19. Yoneyama, M. *et al.* The RNA helicase RIG-I has an essential function in double-stranded RNA–induced innate antiviral responses. *Nat. Immunol.* **5**, 730–737 (2004).
20. Tareen, S.U. & Emerman, M. Human Trim5α has additional activities that are uncoupled from retroviral capsid recognition. *Virology* **409**, 113–120 (2011).
21. Sen, G.C. & Fensterl, V. Crystal structure of IFIT2 (ISG54) predicts functional properties of IFITs. *Cell Res.* **22**, 1407–1409 (2012).
22. Honda, K. *et al.* IRF-7 is the master regulator of type-I interferon–dependent immune responses. *Nature* **434**, 772–777 (2005).
23. Ma, Y. *et al.* Anticancer chemotherapy-induced intratumoral recruitment and differentiation of antigen-presenting cells. *Immunity* **38**, 729–741 (2013).
24. Brahmer, J.R. *et al.* Safety and activity of anti–PD-L1 antibody in patients with advanced cancer. *N. Engl. J. Med.* **366**, 2455–2465 (2012).
25. Foloppe, J. *et al.* Targeted delivery of a suicide gene to human colorectal tumors by a conditionally replicating vaccinia virus. *Gene Ther.* **15**, 1361–1371 (2008).
26. Barbalat, R., Ewald, S.E., Mouchess, M.L. & Barton, G.M. Nucleic acid recognition by the innate immune system. *Annu. Rev. Immunol.* **29**, 185–214 (2011).
27. Goubau, D., Deddouche, S. & Reis, E.S.C. Cytosolic sensing of viruses. *Immunity* **38**, 855–869 (2013).
28. Crawford, M.A. *et al.* Interferon-inducible CXC chemokines directly contribute to host defense against inhalational anthrax in a murine model of infection. *PLoS Pathog.* **6**, e1001199 (2010).
29. Iwamoto, T. *et al.* Gene pathways associated with prognosis and chemotherapy sensitivity in molecular subtypes of breast cancer. *J. Natl. Cancer Inst.* **103**, 264–272 (2011).
30. Tabchy, A. *et al.* Evaluation of a 30-gene paclitaxel, fluorouracil, doxorubicin, and cyclophosphamide chemotherapy response predictor in a multicenter randomized trial in breast cancer. *Clin. Cancer Res.* **16**, 5351–5361 (2010).
31. Hatzis, C. *et al.* A genomic predictor of response and survival following taxane-anthracycline chemotherapy for invasive breast cancer. *J. Am. Med. Assoc.* **305**, 1873–1881 (2011).
32. Desmedt, C. *et al.* Multifactorial approach to predicting resistance to anthracyclines. *J. Clin. Oncol.* **29**, 1578–1586 (2011).
33. Horak, C.E. *et al.* Biomarker analysis of neoadjuvant doxorubicin/cyclophosphamide followed by ixabepilone or Paclitaxel in early-stage breast cancer. *Clin. Cancer Res.* **19**, 1587–1595 (2013).
34. Popovici, V. *et al.* Effect of training-sample size and classification difficulty on the accuracy of genomic predictors. *Breast Cancer Res.* **12**, R5 (2010).
35. Allred, D.C., Harvey, J.M., Berardo, M. & Clark, G.M. Prognostic and predictive factors in breast cancer by immunohistochemical analysis. *Mod. Pathol.* **11**, 155–168 (1998).
36. Arriagada, R. Results of two randomized trials evaluating adjuvant anthracycline-based chemotherapy in 1146 patients with early breast cancer. *Acta Oncol.* **44**, 458–466 (2005).
37. Spielmann, M. *et al.* Trastuzumab for patients with axillary-node–positive breast cancer: results of the FNCLCC-PACS 04 trial. *J. Clin. Oncol.* **27**, 6129–6134 (2009).
38. MacMicking, J.D. Interferon-inducible effector mechanisms in cell-autonomous immunity. *Nat. Rev. Immunol.* **12**, 367–382 (2012).
39. Alexopoulou, L., Holt, A.C., Medzhitov, R. & Flavell, R.A. Recognition of double-stranded RNA and activation of NF-κB by Toll-like receptor 3. *Nature* **413**, 732–738 (2001).
40. Tatematsu, M., Nishikawa, F., Seya, T. & Matsumoto, M. Toll-like receptor 3 recognizes incomplete stem structures in single-stranded viral RNA. *Nat. Commun.* **4**, 1833 (2013).
41. Shatz, M., Menendez, D. & Resnick, M.A. The human TLR innate immune gene family is differentially influenced by DNA stress and p53 status in cancer cells. *Cancer Res.* **72**, 3948–3957 (2012).
42. Bernard, J.J. *et al.* Ultraviolet radiation damages self noncoding RNA and is detected by TLR3. *Nat. Med.* **18**, 1286–1290 (2012).
43. Van, D.N. *et al.* Innate immune agonist, dsRNA, induces apoptosis in ovarian cancer cells and enhances the potency of cytotoxic chemotherapeutics. *FASEB J.* **26**, 3188–3198 (2012).
44. Ellermeier, J. *et al.* Therapeutic efficacy of bifunctional siRNA combining TGF-β1 silencing with RIG-I activation in pancreatic cancer. *Cancer Res.* **73**, 1709–1720 (2013).
45. Salaun, B. *et al.* TLR3 as a biomarker for the therapeutic efficacy of double-stranded RNA in breast cancer. *Cancer Res.* **71**, 1607–1614 (2011).
46. Conforti, R. *et al.* Opposing effects of toll-like receptor (TLR3) signaling in tumors can be therapeutically uncoupled to optimize the anticancer efficacy of TLR3 ligands. *Cancer Res.* **70**, 490–500 (2010).
47. Schreiber, R.D., Old, L.J. & Smyth, M.J. Cancer immunoediting: integrating immunity's roles in cancer suppression and promotion. *Science* **331**, 1565–1570 (2011).
48. Vesely, M.D., Kershaw, M.H., Schreiber, R.D. & Smyth, M.J. Natural innate and adaptive immunity to cancer. *Annu. Rev. Immunol.* **29**, 235–271 (2011).
49. Lenci, R.E. *et al.* Influence of genetic variants in type I interferon genes on melanoma survival and therapy. *PLoS ONE* **7**, e50692 (2012).
50. Fuertes, M.B. *et al.* Host type I IFN signals are required for antitumor $CD8^+$ T cell responses through $CD8\alpha^+$ dendritic cells. *J. Exp. Med.* **208**, 2005–2016 (2011).
51. Diamond, M.S. *et al.* Type I interferon is selectively required by dendritic cells for immune rejection of tumors. *J. Exp. Med.* **208**, 1989–2003 (2011).
52. Harlin, H. *et al.* Chemokine expression in melanoma metastases associated with $CD8^+$ T-cell recruitment. *Cancer Res.* **69**, 3077–3085 (2009).
53. Hong, M. *et al.* Chemotherapy induces intratumoral expression of chemokines in cutaneous melanoma, favoring T-cell infiltration and tumor control. *Cancer Res.* **71**, 6997–7009 (2011).
54. Eggermont, A.M. *et al.* Ulceration and stage are predictive of interferon efficacy in melanoma: results of the phase III adjuvant trials EORTC 18952 and EORTC 18991. *Eur. J. Cancer* **48**, 218–225 (2012).
55. Ruffell, B. *et al.* Leukocyte composition of human breast cancer. *Proc. Natl. Acad. Sci. USA* **109**, 2796–2801 (2012).
56. Gu-Trantien, C. *et al.* $CD4^+$ follicular helper T cell infiltration predicts breast cancer survival. *J. Clin. Invest.* **123**, 2873–2892 (2013).
57. Denkert, C. *et al.* Tumor-associated lymphocytes as an independent predictor of response to neoadjuvant chemotherapy in breast cancer. *J. Clin. Oncol.* **28**, 105–113 (2010).
58. Weichselbaum, R.R. *et al.* An interferon-related gene signature for DNA damage resistance is a predictive marker for chemotherapy and radiation for breast cancer. *Proc. Natl. Acad. Sci. USA* **105**, 18490–18495 (2008).
59. Chan, S.R. *et al.* STAT1-deficient mice spontaneously develop estrogen receptor α–positive luminal mammary carcinomas. *Breast Cancer Res.* **14**, R16 (2012).
60. Yang, X. *et al.* Targeting the tumor microenvironment with interferon-β bridges innate and adaptive immune responses. *Cancer Cell* **25**, 37–48 (2014).

ONLINE METHODS

Reagents and kits. Monoclonal antibodies specific for murine Ifnar1 (clone MAR1-5A3)[61] and Cxcr3 (clone 173)[62] for *in vitro* and *in vivo* depletion experiments were provided by R.D.S. Murine IgG1 antibodies (isotype-matched controls) were purchased from R&D Systems (Minneapolis, MN, USA). Ifn-αβ–neutralizing antibodies as well as high-titer, purified mouse Ifn-αβ (1.5×10^6 U mg^{-1} protein) were produced in house, as reported previously[63,64]. Supernatants from untreated L929 cells were employed as a negative control for purified Ifn-αβ (mock). Recombinant mouse Ifn-α1 was a kind gift from G. Schiavoni and G. D'Agostino, recombinant mouse Ifn-γ was from PeproTech (Rocky Hill, NJ, USA), and recombinant mouse Cxcl10 (also known as Ip-10 or Grg-2) and recombinant mouse Ccl4 (also known as Mip-1β) were from R&D Systems. DX, mitoxantrone dihydrochloride, CDDP and mitomycin C were from Sigma-Aldrich (St. Louis, MO, USA), and oxaliplatin was from Teva Pharmaceutical Industries (the Netherlands). Benzonase nuclease and RNase H were from Sigma-Aldrich, and RNase A and DNase I were from Calbiochem (Darmstadt, Germany). ELISA kits specific for mouse Ifn-β, Ccl3, Ccl5 and Cxcl10 were purchased from PBL Interferon Source (Piscataway, NJ, USA) or R&D Systems.

Cell lines, tumor cell clones and culture conditions. Unless otherwise indicated, media and supplements for cell culture were purchased from Gibco-Invitrogen (Carlsbad, CA, USA), and plasticware was from Corning B.V. Life Sciences (Amsterdam, the Netherlands). All cells were maintained in standard culture conditions (37 °C, 5% CO_2). WT mouse fibrosarcoma MCA205 cells (H-2^b) and their GFP-expressing, *Ifnar1*$^{-/-}$, *Tlr3*$^{-/-}$ and *Rnasel*$^{-/-}$ derivatives, MCA205-derived tumor clones, WT, *Ifnar2*$^{-/-}$, *Tlr3*$^{-/-}$, *Ticam1*$^{-/-}$ and *Ifih1*$^{-/-}$ mouse leukemia L1210S61 cells, 4T1 and AT3 breast carcinoma cells and 1-5 and 2-9 mouse NSCLC cells were cultured in RPMI 1640 medium supplemented with 10% (v/v) FBS, 2 mM L-glutamine, 100 IU ml^{-1} penicillin G sodium salt, 100 μg ml^{-1} streptomycin sulfate, 1 mM sodium pyruvate, 1 mM non-essential amino acids and 1 mM 4-(2-hydroxyethyl)-1-piperazineethanesulfonic acid (HEPES) buffer. OVA-expressing mouse melanoma B16 (B16.OVA) cells were cultured in RPMI medium supplemented as described above plus 0.4 mg ml^{-1} Geneticin (G418, Calbiochem). Human breast carcinoma MDA-MB-231 and HCC-1937 cells were cultured in DMEM supplemented as described above. *Ifnar1*$^{-/-}$, *Tlr3*$^{-/-}$ and *Rnasel*$^{-/-}$ MCA205 cell lines were generated using the CompoZr Zinc Finger Nuclease Technology (CKOZFND33654, CKOZFND42896 and CKOZFND40292, Sigma-Aldrich), as per the manufacturer's recommendations[65].

Cytofluorometric quantification of cell death. Cell death was assessed using the FITC-Annexin V detection Kit I (BD Biosciences, San José, CA, USA) following standard procedures[66–68]. Briefly, 1×10^5 cells per sample were collected, washed in PBS, pelleted and resuspended in incubation buffer (10 mM HEPES-NaOH, pH 7.4, 140 mM NaCl and 5 mM $CaCl_2$) supplemented with FITC- or allophycocyanin-conjugated annexin V. Samples were then incubated in the dark for 15 min, followed by the addition of 400 μl incubation buffer supplemented with 0.1% DAPI (Life Technologies Inc., Carlsbad, CA, USA). Acquisitions were performed on a FACSCalibur (Becton Dickinson, San José, CA, USA) or Cyan (Beckman Coulter, Brea, CA, USA) cytofluorometer, and data were statistically evaluated using FlowJo software 7.6.3 (Tree Star, Ashland, OR, USA).

Nuclease exposure. Cancer cell lines were cultured in the presence of anthracyclines alone or in combination with 20 U ml^{-1} Benzonase, 100 U ml^{-1} DNase, 10 U ml^{-1} RNase A or 10 U ml^{-1} RNase H for 3, 6, 12 or 24 h. Thereafter, untreated cells were introduced into the system for 12–24 h. Such recipient cells were analyzed for the expression of ISG products by qRT-PCR and ELISA.

RT-PCR. Total RNA extraction and genomic DNA removal were performed with the RNeasy Mini Kit (Qiagen, Hilden, Germany) following the manufacturer's instructions. Total RNA (1 μg from each sample) was then reverse transcribed into cDNA with the SuperScript III Reverse Transcriptase, RNasin Plus RNase Inhibitor (Life Technologies, Saint Aubin, France) in the presence of random primers (Promega, Charbonnieres, France) and the Deoxynucleoside Triphosphate Set, PCR grade (Roche Diagnostics, Meylan, France). Expression of IFN-related genes and chemokine genes was analyzed with TaqMan Gene Expression Assays using Universal Master Mix II on a StepOnePlus Real-Time PCR System (Life Technologies, France). qRT-PCR data were invariably normalized to the expression levels of the housekeeping gene *Ppia* (peptidylprolyl isomerase A).

Immunoblotting. Immunoblotting was performed according to standard procedures[67,69]. In brief, cells were washed twice with ice-cold PBS and lysed in an aqueous solution containing 1% NP-40, 20 mM HEPES (pH 7.9), 10 mM KCl, 1 mM EDTA, 10% glycerol, 1 mM orthovanadate, 1 mM PMSF, 1 mM dithiothreitol and commercial protease inhibitors. Whole-cell lysates were separated on 4–12% polyacrylamide NuPAGE Novex Bis-Tris gels (Life Technologies Inc.), electrotransferred to polyvinylidene fluoride membranes (Bio-Rad, Hercules, CA, USA) and incubated with primary antibodies specific for murine Ifih1, (clone D74E4, 1:1,000 diluted, Cell Signaling Technology, Danvers, USA), Rnasel (clone H300 sc-25798, 1:200 diluted, Santa Cruz, USA) and Tlr3 (clone ab13915, 1:1,000 diluted, Abcam, USA). Equal lane loading was monitored by probing membranes with a glycerhaldeyde-3-phosphate dehydrogenase (Gapdh)-specific antibody (mouse monoclonal IgG_1 #MAB374, 1:300 diluted, Millipore-Chemicon International, Temecula, CA, USA). Membranes were revealed with suitable horseradish peroxidase conjugates (SouthernBiotech, Birmingham, AL, USA), followed by chemiluminescence-based detection with the SuperSignal West Pico reagent (Thermo Scientific-Pierce, Rockford, IL, USA) and the ImageQuant LAS 4000 software-assisted imager (GE Healthcare, Piscataway, NJ, USA).

Animals. Mice were maintained in specific pathogen–free conditions in a temperature-controlled environment with 12-h light, 12-h dark cycles and received food and water *ad libitum*. Animal experiments followed the Federation of European Laboratory Animal Science Association (FELASA) or National Health and Medical Research Council of Australia (NH&MRC) guidelines, were in compliance with EU Directive 63/2010 and were approved by the Ethical Committee of the Gustave Roussy Cancer Campus (Villejuif, France), the Istituto Superiore di Sanità (Rome, Italy) or the Peter MacCallum Cancer Centre (Melbourne, Australia). 6- to 7-week-old female WT C57BL/6 (H-2^b) mice were obtained from Harlan France (Gannat, France), Janvier (Le Genest St. Isle, France) and Charles River Laboratories (Saint-Germain sur l'Arbresle, France). 6- to 7-week-old female *Ifnar1*$^{-/-}$ C57BL/6 (H-2^b) mice were kindly provided by the University of Montpellier (Montpellier, France) and the Peter MacCallum Cancer Centre. All mouse experiments were randomized and blinded and sample sizes were calculated to detect a statistically significant effect.

Tumor models, chemotherapy and antitumor vaccination. Eight hundred thousand MCA205 or AT3 cells or 1×10^7 WT, *Ifnar2*$^{-/-}$, *Tlr3*$^{-/-}$ or *Ifih1*$^{-/-}$ MCA205 cells were inoculated subcutaneously (near the thigh) into WT or *Ifnar1*$^{-/-}$ C57BL/6 (H-2^b) mice, and tumor surface (longest dimension × perpendicular dimension) was routinely monitored using a common caliper. When the tumor surface reached 35–45 mm^2, mice received either 2.9 mg per kg body weight. DX or 150 mg per kg body weight CDDP i.t. in 50 μl of PBS or an equivalent volume of PBS either alone or in combination with 2×10^4 U per mouse recombinant Ifn-αβ i.t., 1 μg per mouse recombinant Cxcl10 i.t., 1 μg per mouse recombinant Ccl4 i.t. or 2.5 mg per mouse Ifnar1-specific antibodies intraperitoneally (i.p.). For vaccination experiments, 1×10^6 MCA205 or B16.OVA cells were left untreated or treated with 25 μM DX or 150 μM CDDP alone or combined with 1,000 U ml^{-1} recombinant Ifn-αβ, 0.1 μg ml^{-1} recombinant Cxcl10, 0.1 μg ml^{-1} recombinant Ccl4, 10 ng ml^{-1} recombinant Ifn-γ, 200 U ml^{-1} Ifn-αβ–specific antibodies or 10 μg ml^{-1} Ifnar1-specific antibodies for 24 h, resulting in approximately 40% cell death (assessed as described above), and were then subcutaneously inoculated (in 200 μl PBS) into the lower flanks of 6-week-old female C57BL/6 mice. Two hundred thousand untreated control cells of the same type were inoculated into the opposite flank 10 d later, and tumor growth was monitored weekly. The absence of tumors was considered an indication of efficient antitumor vaccination. Animals bearing neoplastic lesions that exceeded 20–25% of their body mass were euthanized. All experiments contained 5 to 10 mice per group and were run at least 2 to 4 times, yielding similar results.

doi:10.1038/nm.3708

Tumor dissection and sorting. Tumors from mice receiving PBS or DX were carefully removed 2, 4 and 8 d after treatment, cut into small pieces with scissors within digesting buffer (400 U ml^{-1} collagenase IV and 200 U ml^{-1} DNase I in RPMI 1640 medium) and incubated for 30 min at 37 °C. Single-cell suspensions obtained by grinding digested tissues and filtering them through a 70-µm cell strainer were purified based on CD45 expression with the CD45 Cell Isolation Kit and an AutoMACS Separator (both from Miltenyi Biotec, Bergisch Gladbach, Germany) using proprietary programs. After washing in PBS, cells were resuspended at 1×10^7 cells ml^{-1} and processed, either as such or after cytofluorometric isolation of various $CD45^+CD3^-CD19^-CD11b^+$ cell subsets, for transcriptional or functional assays. The indirect immunofluorescence staining protocol and gating strategy for the isolation of specific $CD45^+CD3^-CD19^-CD11b^+$ cell populations have been described in detail previously[15,23]. The fluorescence-activated sorting of GFP-expressing or stained cells was carried out on a FACSVantage sorter (Becton Dickinson). DAPI was employed in all experiments to discriminate between live and dead cells. The purity of isolated cells was normally >95%.

Microarray analyses with Illumina whole-genome arrays. Total RNA was isolated from the $CD45^+$ and $CD45^-$ fractions of tumors collected before treatment (T0) or 2 (T2) or 8 (T8) d later from three mice per group. Biotin-labeled cRNA preparations were obtained using the Illumina TotalPrep RNA Amplification Kit (Applied Biosystems-Life Technologies Inc., Carlsbad, CA, USA), as recommended by the manufacturer. Thereafter 1.5 µg cRNA was hybridized to Illumina Sentrix Mouse-6 v.1 BeadChips, which were scanned with an Illumina BeadStation 500 (both from Applied Biosystems-Life Technologies Inc.). Data were collected with Illumina BeadStudio 3.1.1.0 software, and statistical analyses were conducted on the IlluminaGUI R-package[15,70] (accession code: GSE46275).

Patients included in neoadjuvant chemotherapy studies. Patients for gene expression analyses were selected among 591 individuals who received preoperative anthracycline-based, taxane-free chemotherapeutic regimens at the Gustave Roussy Cancer Campus between 1987 and 2003. Inclusion criteria consisted of pCR, defined as the disappearance of the invasive component of the primary lesion and the absence of cancer cells in axillary lymph nodes after chemotherapy, and the availability of frozen, pretreatment samples for molecular studies. Twenty-six cases were identified, and 26 additional cases were selected as controls. Controls included individuals with tumors that were relatively resistant to chemotherapy, defined as <75% clinical response and residual disease at post-chemotherapy pathologic examination, and matched for ER status. The biopsy specimens of two cases experiencing pCR yielded RNA of poor quality and were therefore excluded from the analysis. A double check of clinical characteristics revealed that one patient achieving pCR actually received two cycles of docetaxel in addition to four courses of anthracyclines. This patient was retained in the analysis. The study was approved by the local Institutional Reviewing Board at the Institut Gustave Roussy (Villejuif, France). All patients signed an informed consent form for the storage and molecular analysis of their samples.

In addition, 41 patients with newly diagnosed, biopsy-proven, stage II or IIIA $ERBB2^-$ BC were evaluated in a prospective study of neoadjuvant anthracycline-based chemotherapy at Georges François Leclerc Cancer Center (Dijon, France). Thirty-three patients underwent two serial biopsies, one at diagnosis (T0) and a second 3 weeks after the first cycle of chemotherapy (T1). A total of 74 biopsies (33 pairs taken at T0 and T1, four unpaired taken at T0 only and four unpaired taken at T1 only) were available for immunohistochemical assessment of MX1 expression. This prospective study was approved by the Institutional Review Board at the Georges François Leclerc Cancer Center (Dijon, France), and all women gave their informed consent.

Publicly available patient cohorts testing neoadjuvant chemotherapy. By searching public databases (PubMed, Gene Expression Omnibus and ArrayExpress) in December 2013 for the keywords 'breast carcinoma', 'preoperative chemotherapy' or 'neoadjuvant chemotherapy' (including anthracyclines alone or combined with taxanes), we identified six studies published in peer-reviewed journals that performed gene expression studies on tumor biopsies obtained at diagnosis and for which pCR data were available (GSE6861 and refs. 30–33,71, accession codes GSE20271, GSE25065, GSE16446 and GSE41998). pCR was always defined as the disappearance of the invasive component of the primary tumor and the absence of invasive malignant lesions in the axillary nodes, with the single exception of the study by Tabchy *et al.*[30], in which patients exhibiting minimal residual disease were also considered as responders. We excluded from the analysis trastuzumab-pretreated $ERBB2^+$ patients.

Patients included in the randomized adjuvant chemotherapy study. Two French multicentric randomized trials compared adjuvant anthracycline-based chemotherapy with no chemotherapy in pre- and post-menopausal patients with early BC between 1989 and 1995, including a total of 1,146 patients. Nine hundred and thirty-five (83%) of these patients were followed at the Gustave Roussy Cancer Campus (Villejuif, France). The inclusion criteria and results of this clinical trial have been reported previously[36]. Of 935 patients, 688 were post-menopausal and presented with either histologically confirmed axillary lymph node involvement or no lymph node involvement but grade II/III disease. The remaining 247 patients were pre-menopausal and presented with no axillary lymph node involvement but grade II/III disease. All patients gave their informed consent prior to inclusion in the study, and the Ethics Committee in Kremlin-Bicêtre, France, approved both protocols.

Eligible patients who agreed to participate in the study were allocated randomly to no adjuvant chemotherapy (the observation group in **Fig. 6**) or six courses of anthracycline-based chemotherapy (the chemotherapy group in **Fig. 6**). The chemotherapy regimen consisted of six courses of 500 mg m^{-2} 5-fluorouracil, 50 mg m^{-2} doxorubicin (FAC50 regimen) or epirubicin (FEC50 regimen) and 500 mg m^{-2} cyclophosphamide administered intravenously (i.v.) on day 1 of 28-d cycles. Survival data were updated in December 2009. The FEC50 regimen was used in 91% of the patients included in the present analysis.

Patients included in the PACS04 adjuvant trial. We analyzed 497 tissue microarrays from the PACS04 phase 3 clinical trial (ClinicalTrials.gov ID NCT00054587), enrolling 3,010 patients with BC presenting with axillary lymph node involvement but no distant metastases between 2001 and 2004. This randomized study compared six cycles of 500 mg m^{-2} 5-fluorouracil, 50 mg m^{-2} epirubicin and 500 mg m^{-2} cyclophosphamide administered i.v. on day 1 of 21-d cycles (FEC100 regimen) with six cycles of 75 mg m^{-2} epirubicin and 775 mg m^{-2} docetaxel (ED75 regimen). Radiotherapy was administered after conservative surgery, and hormonotherapy was prescribed to patients with ER- or progesterone receptor (PR)-positive tumors. Patients overexpressing ERBB2 (19%) were further randomized to either 1 year of trastuzumab-based chemotherapy or observation. The ED75 regimen conveyed no benefits in terms of disease-free survival or OS as compared with the standard FEC100 protocol. Surgical specimens were available for 1,836 out of 3,010 participants in the study. These samples were collected centrally in the context of the UNICANCER initiative by the Department of Pathology of the Jean Perrin Cancer Center (Clermont-Ferrand, France) and were included in tumor TMAs. Quality-control criteria and specimen availability account for the assessment of MX1 expression in 484 samples only. Indeed, 327 TMAs were analyzed for both MX1 and TLR3 expression, with 487 and 337 TMAs analyzed for MX1 and TLR3 expression individually, respectively. In three cases analyzed for MX1 expression, tumor grade was not annotated. The PACS04 protocol was reviewed and approved by the ethics committee/institutional review board, and the study was conducted according to the Declaration of Helsinki and European Good Clinical Practice requirements. Patients signed an informed consent.

TMA construction. Formalin-fixed, paraffin-embedded (FFPE) surgical specimens from patients with BC were retrieved from the UNICANCER tumor bank. H&E-stained slides corresponding to each sample were reviewed by a pathologist to identify neoplastic areas. TMAs were constructed using tissue cores with a diameter of 0.6 mm from representative malignant areas. Such cores were transferred to a paraffin block using a semiautomated TMA-building instrument (Alphelys, Plaisir, France). Triplicate tumor cores were taken from each specimen, resulting in composite TMA blocks containing samples from 1,836 out of 3,010 (61%) patients enrolled in the PACS04 trial. Normal breast tissues were also included in TMAs as control material. All donors gave informed consent for use of these samples, including the normal controls. Along similar lines,

a TMA was constructed from the primary neoplastic lesions of 824 out of 935 (88%) patients participating in the clinical trials organized by the Gustave Roussy Cancer Campus. This TMA also contained three replicate spots for each primary tumor. Multiple 3-µm-thick sections were cut for H&E staining as well as for the immunohistochemical detection of TLR3 and human MX1.

Immunohistochemical detection of TLR3 and MX1. Murine antibodies specific for human TLR3 (clone 40F9.6) and human MX1 (polyclonal) were from Innate Pharma (Marseille, France) and Sigma-Aldrich (St. Louis, MO, USA), respectively. For the immunohistochemical detection of TLR3, 3-µm-thick sections from FFPE human breast carcinoma specimens were mounted on poly-L-lysine–coated slides, deparaffinized and hydrated though a series of graded alcohols to water. Sections were pretreated with 0.01 M sodium citrate buffer (pH 6.0; Zymed-Life Technologies Inc., Carlsbad, CA, USA) for 20 min in a 98 °C water bath. Endogenous peroxidase activity was inhibited by treating slides with 3% hydrogen peroxidase (DAKO, Glostrup, Denmark) for 10 min, followed by incubation with 10 µg ml^{-1} 40F9.6 (anti-TLR3) antibodies for 1 h at room temperature. Visualization was performed using the EnVision system and 3,3′-diaminobenzidine (DAB), both from DAKO, according to the manufacturer's instructions. Sections were counterstained with Mayer's hematoxylin (Sigma-Aldrich). Controls for staining specificity were processed in the same manner but substituting the 40F9.6 antibodies with 10 µg ml^{-1} murine IgG1 antibodies. The immunohistochemical assessment of MX1 was performed on a BenchMark ULTRA automated immunostainer (Ventana, Tucson, AZ, USA). Antigen retrieval was performed by incubating slides in EDTA buffer (pH 8.0) for 36 min at 95 °C. Subsequently, slides were incubated with the MX1 antibody diluted 1:100 in commercial diluent (Zymed, San Francisco, CA, USA) for 1 h at 37 °C. MX1 detection and counterstaining were performed with the biotin-free peroxidase-base UltraView Universal DAB Detection Kit and a commercial Hematoxylin Kit, respectively, both from Ventana. A section of mesothelium was employed as a positive staining control, and negative controls were provided by slides processed similarly as the test samples but in the absence of primary MX1 antibodies. Only MX1 expression by cancer cells was taken into account for the purpose of this study. Staining intensity and the percentage of stained cancer cells were combined to generate a cumulative score for the Allred system[35]. A case was considered as positive for MX1 expression if the Allred score was >6. This cutoff value was derived from the analysis of 24 cases for which both the *MX1* metagene score, as determined by gene expression analysis, and MX1 expression levels, as assessed by immunohistochemistry, were available. This approach demonstrated that an Allred score of six was the optimal cutoff to distinguish neoplasms with high versus low *MX1* metagene score in our study.

Gene expression profiling. Frozen samples from patients treated with neoadjuvant chemotherapy were profiled on gene expression microarrays. Total RNA was extracted using the RNeasy Mini Kit (Qiagen, Hilden, Germany). The amount and quality of purified RNA were assessed with a DU-640 ultraviolet spectrophotometer (Beckman Coulter) and were considered adequate for further analyses if the optical density at 260 nm (OD_{260}) to OD_{280} ratio was >1.8 and the total RNA yield was >1 µg. All 50 case-control samples yielded adequate RNA and were profiled on Affymetrix U133A gene chips at the University of Texas MD Anderson Cancer Center using a standard operating procedure[70] (accession code: GSE22093).

Statistical analyses. dCHIP v. 1.3 (http://www.hsph.harvard.edu/cli/complab/dchip/) software was used to generate probe-level gene expression intensities and quality measures, including median intensity, percentage of probe set outliers and percentage of single probe outliers for each chip. This program normalizes all arrays to one standard array representing a chip with the median overall intensity. The reference chip and normalization procedure are available online at http://bioinformatics.mdanderson.org/pubdata.html. Normalized gene expression values were transformed to a $\log_2$ scale for analysis and are available at ArrayExpress under accession code GSE22093. We tested the predictive values of nine different metagenes representative of biological processes or cell differentiation (IFN response, proliferation, stromal reaction, B cell, T cell, ER, apocrine, adipocyte and hypoxia). These metagenes have been tested previously as predictors of response to neoadjuvant anthracycline-containing chemotherapy[29]. Each of these metagenes contains 50 genes that are highly coexpressed with a central anchor gene, after which the metagene was named. Metagene scores were computed as the average expression levels of member genes. **Supplementary Table 3** lists all the genes and corresponding U133A probe sets defining the nine metagenes examined in this study. The predictive performance of molecular variables was examined using the AUC method, and 95% CIs were estimated based on bootstrap sampling with 10,000 iterations. The Benjamini and Hochberg procedure was used to adjust *P* values for multiple testing. To calculate the optimal sensitivity, specificity and positive and negative predictive values, the Youden point on the ROC curve was determined. The Youden point corresponds to the point on the ROC curve that is farthest from chance and defines predictor thresholds that maximize both the sensitivity and the specificity while minimizing misclassification rates in a given data set. Data analyses were carried out in the R v. 3.0.1 environment (http://www.r-project.org/). A Cox model was used to adjust for the significant prognostic clinical factors (histological grade, lymph node involvement and ER status). Treatment effects according to ER status and MX1 staining were analyzed by testing the interaction between treatment and each variable. Survival curves were determined by the Kaplan-Meier method. The incidences of markers across clinical parameters were estimated using logistic regression and are reported as odds ratio alongside 95% CIs and *P* values. The combined values of Pearson's correlation coefficients were computed considering the weighted average for each gene, with the weights proportional to the cohort sizes. For the IFN module score, the combined *P* value of response, based on the Fisher's method, was 5.5×10^{-7}. Pairwise statistical comparisons and tumor growth curves were performed using unpaired, two-tailed Student's *t* test, and Kaplan-Meier curves were compared with the log-rank test. Unless otherwise specified, the threshold for statistical significance was set to $P < 0.05$.

61. Sheehan, K.C. *et al.* Blocking monoclonal antibodies specific for mouse IFN-α/β receptor subunit 1 (IFNAR-1) from mice immunized by *in vivo* hydrodynamic transfection. *J. Interferon Cytokine Res.* **26**, 804–819 (2006).
62. Uppaluri, R. *et al.* Prolongation of cardiac and islet allograft survival by a blocking hamster anti-mouse CXCR3 monoclonal antibody. *Transplantation.* **86**, 137–147 (2008).
63. Gresser, I., Tovey, M.G., Maury, C. & Bandu, M.T. Role of interferon in the pathogenesis of virus diseases in mice as demonstrated by the use of anti-interferon serum. II. Studies with herpes simplex, Moloney sarcoma, vesicular stomatitis, Newcastle disease, and influenza viruses. *J. Exp. Med.* **144**, 1316–1323 (1976).
64. Tovey, M.G., Begon-Lours, J. & Gresser, I. A method for the large scale production of potent interferon preparations. *Proc. Soc. Exp. Biol. Med.* **146**, 809–815 (1974).
65. Gaj, T., Guo, J., Kato, Y., Sirk, S.J. & Barbas, C.F. III. Targeted gene knockout by direct delivery of zinc-finger nuclease proteins. *Nat. Methods* **9**, 805–807 (2012).
66. Galluzzi, L. *et al.* Guidelines for the use and interpretation of assays for monitoring cell death in higher eukaryotes. *Cell Death Differ.* **16**, 1093–1107 (2009).
67. Galluzzi, L. *et al.* Prognostic impact of vitamin B6 metabolism in lung cancer. *Cell Reports* **2**, 257–269 (2012).
68. Kepp, O., Galluzzi, L., Lipinski, M., Yuan, J. & Kroemer, G. Cell death assays for drug discovery. *Nat. Rev. Drug Discov.* **10**, 221–237 (2011).
69. Criollo, A. *et al.* Mitochondrial control of cell death induced by hyperosmotic stress. *Apoptosis* **12**, 3–18 (2007).
70. Schultze, J.L. & Eggle, D. IlluminaGUI: graphical user interface for analyzing gene expression data generated on the Illumina platform. *Bioinformatics* **23**, 1431–1433 (2007).
71. Antonov, J. *et al.* Molecular risk assessment of BIG 1–98 participants by expression profiling using RNA from archival tissue. *BMC Cancer* **10**, 37 (2010).
72. Gong, Y. *et al.* Determination of oestrogen-receptor status and ERBB2 status of breast carcinoma: a gene-expression profiling study. *Lancet Oncol.* **8**, 203–211 (2007).

doi:10.1038/nm.3708